AEDC-TR-79-85

A Method for Estimating Jet Entrainment Effects on Nozzle-Afterbody Drag

R. C. Bauer
ARO, Inc.

February 1980

Final Report for Period October 1978 — September 1979

Approved for public release; distribution unlimited.

**ARNOLD ENGINEERING DEVELOPMENT CENTER
ARNOLD AIR FORCE STATION, TENNESSEE
AIR FORCE SYSTEMS COMMAND
UNITED STATES AIR FORCE**

NOTICES

This report has been reviewed by the Office of Public Affairs (PA) and is releasable to the National Technical Information Service (NTIS). At NTIS, it will be available to the general public, including foreign nations.

APPROVAL STATEMENT

This report has been reviewed and approved.

Elton R Thompson

ELTON R. THOMPSON
Project Manager
Directorate of Technology

Approved for publication:

FOR THE COMMANDER

Marion L. Laster

MARION L. LASTER
Director of Technology
Deputy for Operations

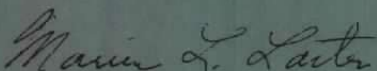| REPORT DOCUMENTATION PAGE		READ INSTRUCTIONS BEFORE COMPLETING FORM
1 REPORT NUMBER AEDC-TR-79-85	2 GOVT ACCESSION NO	3 RECIPIENT'S CATALOG NUMBER
4 TITLE (and Subtitle) A METHOD FOR ESTIMATING JET ENTRAINMENT EFFECTS ON NOZZLE-AFTERBODY DRAG		5 TYPE OF REPORT & PERIOD COVERED Final Report, October 1978 – September 1979
		6 PERFORMING ORG REPORT NUMBER
7 AUTHOR(s) R. C. Bauer, ARO, Inc., a Sverdrup Corporation Company		8 CONTRACT OR GRANT NUMBER(s)
9 PERFORMING ORGANIZATION NAME AND ADDRESS Arnold Engineering Development Center Air Force Systems Command Arnold Air Force Station, Tennessee 37389		10 PROGRAM ELEMENT PROJECT, TASK AREA & WORK UNIT NUMBERS Program Element 65807F
11 CONTROLLING OFFICE NAME AND ADDRESS Arnold Engineering Development Center/DOS Air Force Systems Command Arnold Air Force Station, Tennessee 37389		12 REPORT DATE February 1980
		13 NUMBER OF PAGES 24
14 MONITORING AGENCY NAME & ADDRESS(if different from Controlling Office)		15 SECURITY CLASS (of this report) UNCLASSIFIED
		15a DECLASSIFICATION DOWNGRADING SCHEDULE N/A

16 DISTRIBUTION STATEMENT (of this Report)

Approved for public release; distribution unlimited.

17 DISTRIBUTION STATEMENT (of the abstract entered in Block 20, if different from Report)

18 SUPPLEMENTARY NOTES

Available in the Defense Technical Information Center (DTIC).

19 KEY WORDS (Continue on reverse side if necessary and identify by block number)

interactions	cold jet
jets	transonic
drag	nozzle-afterbody
predictions	wind tunnel testing
hot jet	

20 ABSTRACT (Continue on reverse side if necessary and identify by block number)

A highly simplified analysis was used to derive an expression for estimating the induced afterbody drag caused by the turbulent jet-mixing process. The approach estimates the induced velocity produced by the jet-mixing process and uses small perturbation concepts to estimate the resulting pressure change on the afterbody surface from which the induced afterbody drag coefficient is obtained. The theoretical induced afterbody drag (entrainment drag)

DD FORM 1473 EDITION OF 1 NOV 65 IS OBSOLETE
1 JAN 73

20.   ABSTRACT, Concluded.

is combined with the maximum jet plume diameter blockage condition
to form a correlation method that accounts for the effects of jet
area ratio, exit angle, total temperature, molecular weight and
ratio of specific heats for a given external stream Mach number,
Reynolds number, and afterbody geometry. For verification, the
correlation method was used to predict the drag of an H_2 and C_2H_4
jet from the measured drag of an N_2 jet and to predict the drag of
a hot jet from the measured drag of a cold jet for both the 15- and
25-deg AGARD afterbody configurations in the Mach number range from
0.6 to 1.5. The average accuracy of the correlation method is
better than 10 percent for both afterbody configurations and is 40
to 50 percent more accurate than a correlation method based only on
the blockage parameter. A brief numerical study indicates that the
major parameter which correlates the jet entrainment effect is the
product of the jet gas constant and total temperature.

AFSC
Arnold AFS Tenn

PREFACE

The work reported herein was conducted by the Arnold Engineering Development Center (AEDC), Air Force Systems Command (AFSC). The results of the research were obtained by ARO, Inc., AEDC Division (a Sverdrup Corporation Company), operating contractor for the AEDC, AFSC, Arnold Air Force Station, Tennessee, under ARO Project Number P32A-01A. The Air Force project manager was Mr. E. R. Thompson, AEDC/DOT. The manuscript was submitted for publication on September 1, 1979.

1

CONTENTS

Page

ILLUSTRATIONS

Figure

TABLES

1.0 INTRODUCTION

Wind tunnel tests concerned with engine-airframe integration usually use a cold jet to simulate the effect the real hot jet has on the airframe pressure distribution and resulting afterbody pressure drag. Unfortunately, there is no reliable method available for predicting the cold jet operating condition necessary to simulate a specific hot jet operating condition with respect to afterbody drag. This problem has been studied both experimentally and theoretically for many years. The studies have been primarily concerned with axisymmetric configurations as shown in Fig. 1; however, it is expected that three-dimensional configurations will be studied in the future.

The experimental results presented in Refs. 1 and 2 clearly show that the afterbody drag obtained with a hot jet is significantly less than that obtained with a cold jet operating at the same pressure ratio. The reason for this difference is that both the jet plume shape (blockage) and the turbulent mixing (entrainment) that take place between the jet flow and the external stream can propagate disturbances upstream through the subsonic flow region over the afterbody. In Refs. 1 and 2 it is shown that matching the initial inclination angle of the jet plume is sufficient to correlate the hot and cold jet afterbody drag data for supersonic flow; however, for subsonic and transonic flow an additional correction for the entrainment effect is necessary. In Ref. 3 it is shown that cold jet afterbody drag for an annular jet and various jet nozzle area ratios can be correlated by matching the maximum jet plume diameter rather than the initial inclination angle of the plume. However, some annular jet configurations appear to be strongly influenced by the jet entrainment and require an additional correction. Experiments showing a pure entrainment effect on afterbody drag are presented in Ref. 4. This was accomplished by measuring the drag obtained with both a nitrogen (N_2) jet and a hydrogen (H_2) jet for the same nozzle and afterbody configuration. Because N_2 and H_2 have the same specific heat ratio, the plume blockage effect is identical for equal operating pressures. Thus, the only effect on afterbody drag must be that caused by the difference in jet entrainment. These results show that decreasing the molecular weight of the jet causes the drag to decrease.

The specific characteristic of the jet-mixing process that influences afterbody drag is usually thought to be a displacement of the inviscid jet boundary, which changes the jet plume blockage (Ref. 1). This concept was utilized in the viscous/inviscid analytical technique, presented in Ref. 5, for estimating attached nozzle-afterbody flows. For separated nozzle-afterbody flows, the Chapman-Korst theory, as applied in Ref. 6, suggests an entrainment parameter based on the pumping capacity of the jet plume which involves not only the rate of mixing but also the location of key streamlines. The author has studied

this approach extensively and has found it to be inadequate for subsonic Mach numbers. In this report a theoretical estimate is presented for the drag caused by jet entrainment, based on the induced velocity produced by the turbulent mixing process.

2.0 ANALYSIS

2.1 GENERAL APPROACH

It is well known (Ref. 7) that the turbulent mixing of a jet with an external stream will produce a small induced velocity in the external stream. The magnitude of the induced velocity has been estimated in Ref. 7 to be usually less than 5 percent of the free-stream velocity. Although the induced velocity is small, the corresponding induced pressure on an afterbody results in a significant change in the afterbody drag coefficient. A rough theoretical estimate of the induced drag coefficient can be obtained on the basis of the following assumptions:

1. The induced velocity is a small perturbation, and the resulting pressure change can be computed using the first-order small disturbance equation.

2. The external flow is attached to both the afterbody and the jet plume, and the local external flow velocity is equal to u_∞. Variations in the local stream velocity have been considered and found to have a negligible effect.

3. Over the length of the afterbody, the induced velocity is assumed constant.

4. The induced velocity vector is perpendicular to the average jet plume boundary angle between the jet exit and maximum jet plume position. This angle is taken to be one-half the initial inviscid jet plume angle.

5. The afterbody surface is conical, as shown in Fig. 1, and the induced pressure on the blunt base is the same as that on the afterbody.

6. The operating conditions of the jet are sufficient to produce a maximum jet plume diameter that is equal to or greater than the jet exit diameter.

The induced velocity parallel to the afterbody surface is, by geometry,

$$u' = -v \sin \left[\left(\frac{\Delta\nu + \theta_N}{2} \right) + \theta_B \right] \tag{1}$$

6

The minus sign results from taking the positive direction of v away from the centerline as shown in Fig. 1.
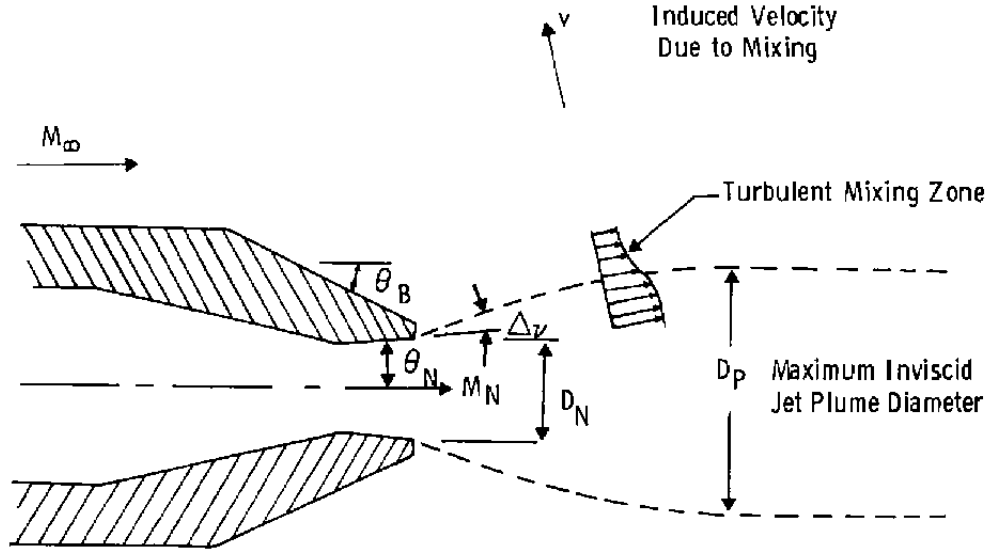
Figure 1. Typical nozzle-afterbody flow field.

From assumption 1 the induced pressure coefficient is

$$C_p = 2\left(\frac{v}{u_\infty}\right) \sin\left[\left(\frac{\Delta\nu - \theta_N}{2}\right) + \theta_B\right]$$ (2)

Therefore, the induced drag coefficient is

$$\Delta C_{DB} = -2\left[1 - \frac{A_N}{A_B}\right]\bar{\phi}\sin\left[\left(\frac{\Delta\nu + \theta_N}{2}\right) + \theta_B\right]$$ (3)

where

$$\bar{\phi} = \frac{v}{u_\infty}$$

The total drag coefficient for the afterbody can be written as

$$C_{DBT} = C_{DBO} + \Delta C_{DB}$$ (4)

where C_{DBO} is the afterbody drag coefficent for $\bar{\phi} = 0$ and, therefore, is only a function of the jet plume blockage. It should be noted that the induced drag coefficient, given by Eq. (3), is also a function of a commonly used blockage parameter, i.e., the initial inclination angle of the jet plume, $(\Delta\nu + \theta_N)$.

2.2 INDUCED VELOCITY

Complex flow fields involving turbulent mixing such as the afterbody flow field shown in Fig. 1 can be analyzed by superimposing on the inviscid flow field an estimate of the turbulent mixing obtained by analyzing a much simpler flow field. This is the basis of the well-known Chapman-Korst component analysis as applied in Refs. 5 and 6. In this report the simpler flow field selected for the turbulent mixing analysis, shown in Fig. 2, consists of an axisymmetric jet in a parallel-flowing external stream. The analytical approach is the same as that presented in Ref. 7 and is based on the following assumptions:

1. The static pressure is constant along the control volume boundary.

2. The initial boundary layers are neglected, and therefore the mixing zone velocity profiles are similar.

3. The width of the mixing zone is small compared to the radius of the jet.

4. The Prandtl, Lewis, and Schmidt numbers are unity.
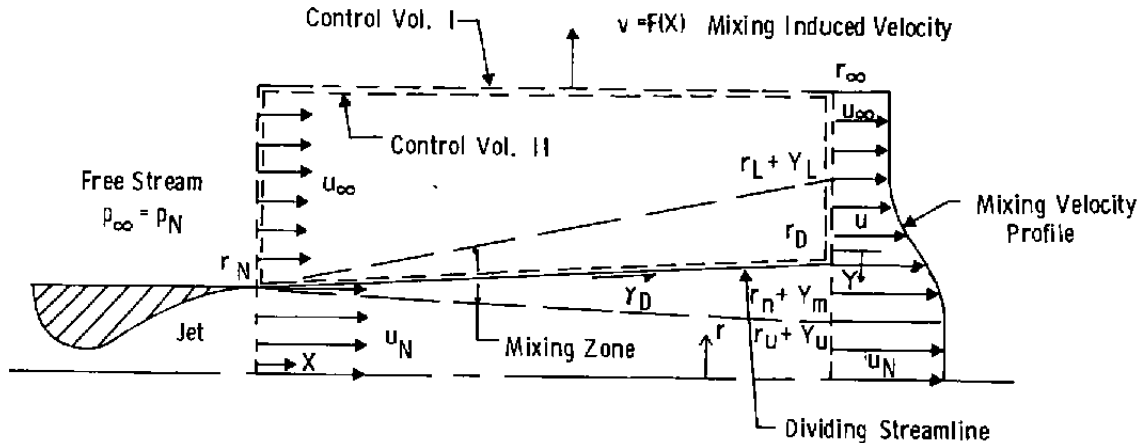

Figure 2. Model for determining the induced velocity due to mixing.

The conservation equations for Control Volume I, shown in Fig. 2, are:

Mass Flow:

$$\rho_N u_N A_N + \rho_\infty u_\infty \left(A_\infty - A_N \right) = 2\pi r_\infty \rho_\infty \int_0^X v dX + \rho_N u_N A_U$$

$$+ 2\pi \int_{r_U}^{r_L} \rho u r dr + \rho_\infty u_\infty \left(A_\infty - A_L \right) \quad (5)$$

8

Momentum:

$$\rho_N u_N^2 A_N - \rho_\infty u_\infty^2 \left(A_\infty - A_N \right) = 2\pi r_\infty \rho_\infty u_\infty \int_0^X v \, dX + \rho_N u_N^2 A_U$$

$$+ 2\pi \int_{r_U}^{r_L} \rho u_1^2 dr + \rho_\infty u_\infty^2 \left(A_\infty - A_L \right) \qquad (6)$$

The unknowns in Eqs. (5) and (6) are the induced velocity, v, and the mixing zone velocity profile shape and size. The mixing velocity profile shape was determined, as in Ref. 7, by solving a highly simplified boundary-layer equation.

$$\phi = \phi_\infty + (1 - \phi_\infty) \phi_0 \qquad (7)$$

where

$$\phi_0 = \tfrac{1}{2} (1 + \text{erf} \, \eta) \qquad (8)$$

and

$$\eta = \frac{\sigma Y}{X} \qquad (9)$$

Thus, the mixing velocity profile is expressed in terms of its own coordinate system, (X,Y), which is shifted relative to the lip of the jet by the distance Y_m, Fig. 2. The nondimensional distance, η_m, is determined from Eqs. (5) and (6) by eliminating the induced velocity term. The final equation is

$$\eta_m = \eta_U - \left[\frac{\left(I_2 \right)_{\eta_U} - \phi_\infty \left(I_1 \right)_{\eta_U}}{1 - \phi_\infty} \right] (1 - C_N^2) \qquad (10)$$

where

$$\left(I_1 \right)_\eta = \int_{-3.0}^\eta \frac{\phi \, d\eta}{\dfrac{R_g}{R_{g_N}} \left[\dfrac{T_t}{T_{t_N}} - \left(\dfrac{C_{p_N}}{C_p} \right) C_N^2 \phi^2 \right]}$$

$$\left(I_2 \right)_\eta = \int_{-3.0}^\eta \frac{\phi^2 \, d\eta}{\dfrac{R_g}{R_{g_N}} \left[\dfrac{T_t}{T_{t_N}} - \left(\dfrac{C_{p_N}}{C_p} \right) C_N^2 \phi^2 \right]}$$

Thus, η_m is independent of X, as are all the properties of the mixing zone when expressed in terms of η. The actual distance Y_m is determined from the definition of η and requires a value for σ, the mixing similarity parameter, which is determined in Section 2.3. In Ref. 7 it is shown that $\eta_u = 3.0$ and $\eta_L = -3.0$ are sufficient for η_m to be independent of the limits of integration. Evaluation of the mass flow and momentum integrals, (I_1) and (I_2), requires local values of the mixture gas constant, R_g, specific heat at constant pressure, C_p, and the total temperature, T_t. The required equations were derived from assumption (4) by the method presented in Ref. 6 and are as follows:

Jet Species Distribution:

$$k = \frac{\phi - \phi_\infty}{1 - \phi_\infty} \tag{11}$$

Gas Constant:

$$\frac{R_g}{R_{g_N}} = k + (1 - k)\frac{R_{g_\infty}}{R_{g_N}} \tag{12}$$

Specific Heat:

$$\frac{C_p}{C_{p_N}} = k + (1 - k)\frac{C_{p_\infty}}{C_{p_N}} \tag{13}$$

Total Temperature:

$$\frac{T_t}{T_{t_N}} = \frac{k + (1 - k)\left(\dfrac{C_{p_\infty}}{C_{p_N}}\right)\left(\dfrac{T_{t_\infty}}{T_{t_N}}\right)}{k + (1 - k)\left(\dfrac{C_{p_\infty}}{C_{p_N}}\right)} \tag{14}$$

Substituting Eq. (5) into Eq. (6) yields

$$\int_o^X v\,dx = \frac{u_\infty Y}{\sigma}\left(\frac{r_N}{r_\infty}\right)\left\{\eta_m - \eta_L + \frac{1}{\phi_\infty}\left(\frac{\rho_N}{\rho_\infty}\right)\left[(\eta_U - \eta_m) - \int_{\eta_L}^{\eta_U}\left(\frac{\rho}{\rho_N}\right)\phi\,d\eta\right]\right\} \tag{15}$$

Differentiating with respect to X yields

$$\frac{v}{u_\infty} = \frac{1}{\sigma}\left(\frac{r_N}{r_\infty}\right)\left\{\eta_m - \eta_L - \frac{1}{\phi_\infty}\left(\frac{\rho_N}{\rho_\infty}\right)\left[(\eta_U - \eta_m) - \left(1 - C_N^2\right)(I_1)_{\eta_u}\right]\right\} \tag{16}$$

Equation (16) shows that the induced velocity, v, is independent of X and varies inversely with the radius, r_∞. However, in this report only the induced velocity along the external stream edge of the mixing zone is of interest, so by assumption 3, $r_\infty \approx r_N$, and Eq. (16) becomes

$$\frac{v}{u_\infty} = \frac{1}{\sigma} \left\{ \eta_m - \eta_L + \frac{1}{\phi_\infty} \left(\frac{\rho_N}{\rho_\infty} \right) \left[\left(\eta_U - \eta_m \right) - \left(1 - C_N^2 \right) \left(I_1 \right)_{\eta_u} \right] \right\} \quad (17)$$

Because the initial boundary layers have been neglected in deriving Eq. (17), the induced velocity, predicted by Eq. (17), near the jet exit will be unrealistically large. To correct for this, the induced velocity predicted by Eq. (17) is arbitrarily reduced by a factor of 0.5. The final equation for the induced velocity to be used in Eq. (3) for estimating the induced drag coefficient is

$$\bar{\phi} = \frac{1}{2\sigma} \left\{ \eta_m - \eta_L + \frac{1}{\phi_\infty} \left(\frac{\rho_N}{\rho_\infty} \right) \left[\left(\eta_u - \eta_m \right) - \left(1 - C_N^2 \right) \left(I_1 \right)_{\eta_U} \right] \right\} \quad (18)$$

The remaining unknown in Eq. (18) is the similarity parameter for turbulent mixing, σ.

2.3 TURBULENT MIXING

The equation for estimating the similarity parameter for turbulent mixing, σ, was derived by applying the method of Ref. 8 to the flow field shown in Fig. 2. The method is simply an application of the flow conservation laws to the Control Volume II, using Prandtl's mixing length hypothesis to represent the turbulent shear stress, τ_D, acting along the dividing streamline. The Conservation equations are as follows:

Mass Flow:

$$\rho_\infty u_\infty \left(A_\infty - A_N \right) = 2\pi r_\infty \rho_\infty \int_0^X v \, dX - 2\pi \int_{r_D}^{r_L} \rho u r dr + \rho_\infty u_\infty \left(A_\infty - A_L \right) \quad (19)$$

Momentum:

$$\rho_\infty u_\infty^2 \left(A_\infty - A_N \right) + 2\pi \int_0^X \tau_D r_D \, dX - 2\pi \int_{r_D}^{r_L} \rho u^2 r dr$$

$$+ \rho_\infty u_\infty^2 \left(A_\infty - A_L \right) + 2\pi r_\infty \rho_\infty u_\infty \int_0^X v \, dX \quad (20)$$

11

The location of the diving streamline is determined by the following equation for conservation of mass flow.

$$\rho_N \, u_N \, A_N \;=\; \rho_N \, u_N \, A_U \;+\; 2\pi \int_{r_U}^{r_D} \rho u r dr \tag{21}$$

These equations are solved on the basis of the four assumptions presented in Section 2.2. Applying the assumptions to Eq. (21) yields

$$\left(I_1 \right)_{\eta_D} = \left(I_1 \right)_{\eta_U} - \frac{(\eta_U - \eta_m)}{\left(1 - C_N^2 \right)} \tag{22}$$

It is important to note that η_D is independent of X; therefore,

$$\phi_D, \left(\frac{d\phi}{d\eta} \right)_D, \; \frac{R_{g_D}}{R_{g_N}}, \; \frac{T_{t_D}}{T_{t_N}} \text{ and } \frac{C_{p_D}}{C_{p_N}}$$

are also independent of X.

Eliminating $\int_0^X v dX$ from Eqs. (19) and (20) yeilds

$$\int_0^X \left(\frac{r_D}{\rho_N \, u_N^2} \right) dX \;=\; \left(\frac{X}{\sigma} \right) \left(1 - C_N^2 \right) \left[\left(I_2 \right)_{\eta_D} - \phi_\infty \left(I_1 \right)_{\eta_D} \right] \tag{23}$$

By Prandtl's mixing length theory,

$$r_D = \rho_D \, \ell_D^2 \left(\frac{du}{dY} \right)_D^2 \tag{24}$$

Now assume that

$$\ell_D = Kb \tag{25}$$

However, by definition,

$$\eta_b = \frac{\sigma b}{\lambda}$$

$$\therefore b = \eta_b \left(\frac{X}{\sigma} \right)$$

and

$$\ell_D = \left(K\eta_b \right) \left(\frac{X}{\sigma} \right) \tag{26}$$

12

Also,

$$\frac{du}{dY} = u_N \left(\frac{d\phi}{d\eta}\right)\left(\frac{d\eta}{dY}\right) = \left(\frac{\sigma u_N}{X}\right)\frac{d\phi}{d\eta} \tag{27}$$

Equation (24) thus becomes

$$\frac{\tau_D}{\rho_N u_N^2} = \left(K\eta_b\right)^2 \left(\frac{\rho_D}{\rho_N}\right)\left(\frac{d\phi}{d\eta}\right)_D^2 \tag{28}$$

Because the fluid dynamic properties along the dividing streamline are independent of X, τ_D, as given by Eq. (28), is also independent of X. Therefore,

$$\int_0^X \left(\frac{\tau_D}{\rho_N u_N^2}\right) dX = \left(\frac{\tau_D}{\rho_N u_N^2}\right) X \tag{29}$$

Substituting Eqs. (28) and (29) into Eq. (23) yields

$$\sigma = \frac{\left(1 - C_N^2\right)\left[\left(I_2\right)_{\eta_D} - \phi_\infty\left(I_1\right)_{\eta_D}\right]}{\left(K\eta_b\right)^2\left(\frac{\rho_D}{\rho_N}\right)\left(\frac{d\phi}{d\eta}\right)_D^2} \tag{30}$$

The remaining unknown in Eq. (30), $K\eta_b$, is determined by applying to Eq. (30) the well-known experimental result (Ref. 9) that $\sigma = 12$ for planar, single-stream, two-dimensional, incompressible mixing. Therefore,

$$\sigma = \frac{\left(\frac{R_{g_D}}{R_{g_N}}\right)\left[\left(\frac{T_D}{T_N}\right) - \left(\frac{C_{p_N}}{C_{p_D}}\right)C_N^2\phi_D^2\right]\left[\left(I_2\right)_{\eta_D} - \phi_\infty\left(I_1\right)_{\eta_D}\right]}{0\ 04235\left(\frac{d\phi}{d\eta}\right)_D^2} \tag{31}$$

3.0 COMPARISON WITH EXPERIMENT

The validity of the theoretical induced drag coefficient cannot be evaluated directly because there are no direct measurements of this drag term. As a result, the theoretical induced drag coefficient was combined with the maximum jet plume diameter blockage parameter of Ref. 3 to form a correlation method that can be applied to a wide variety of experimental data for evaluation. This correlation method accounts for the effects of jet area ratio, exit angle, total temperature, molecular weight and ratio of specific heats on

13

afterbody drag for a given external stream Mach number, Reynolds number, and afterbody geometry. In this report correlation of the effects of the jet thermodynamic properties is the primary concern.

## 3.1 EFFECT OF MOLECULAR WEIGHT

The correlation method was applied to the data of Ref. 4 to predict the drag of an H_2 jet from the measured drag of an N_2 jet. The predicted results are compared with experiment in Figs. 3a, b, and c for the 15-deg AGARD afterbody and in Figs. 4a, b, and c for the 25-deg AGARD afterbody at Mach numbers of 0.6, 0.9, and 1.2, respectively. As shown, the correlation method works well at $M_\infty = 0.6$ for both afterbody configurations but underpredicts the induced drag at $M_\infty = 0.9$ and 1.2 by about the same amount for each afterbody. The afterbody pressure distributions presented in Ref. 4 indicate that the flow is attached at all Mach numbers for the 15-deg afterbody and is attached only at $M_\infty = 0.6$ for the 25-deg afterbody. This indicates that the correlation method is insensitive to the type of flow over the afterbody, which is a desirable characteristic of the method.

The theory indicates that the drag of an N_2 jet is greater than that of an H_2 jet because the induced velocity for the N_2 jet is toward the jet plume (negative) and for the H_2 jet is away from the jet plume (positive). As a result, the induced velocity for the N_2 jet tends to accelerate the flow over the afterbody, decreasing the pressure and increasing the drag, whereas the opposite occurs for the H_2 jet. It is important to note that the direction of the induced velocity, as given by Eq. (18), is independent of the similarity parameter for turbulent mixing, σ, since σ is always positive. Thus, only the magnitude of the induced velocity is determined by the rate of mixing.
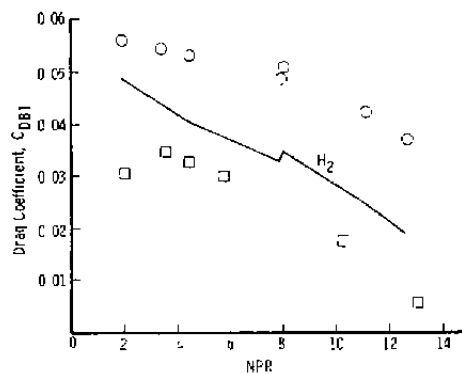
3.2 EFFECT OF THE RATIO OF SPECIFIC HEATS

The correlation method was applied to the data of Ref. 4 to predict the drag of a C_2H_4 (ethylene) jet from the measured drag of an N_2 jet. The predicted results are compared with experiment for both afterbody configurations in Figs. 3a and c and 4a and c for $M_\infty = 0.6$ and 1.2, respectively. As shown, the correlation method agrees well with experiment for both afterbody configurations and Mach numbers. The theoretical induced velocity for the C_2H_4 jet was found to be essentially equal to that for the N_2 jet; thus the difference in drag between the two jets is due to differences in jet plume blockage.
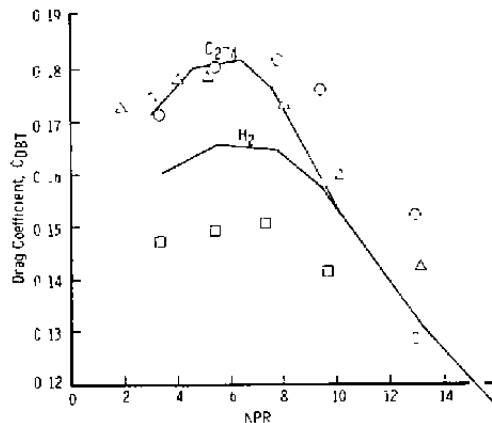
Included in Fig. 3a is a prediction of the drag of an H_2 jet using the measured drag of a C_2H_4 jet. As shown, this predicted drag is essentially equal to that predicted using the measured drag of an N_2 jet, thus verifying that the correlation method is applicable for simultaneous changes in both molecular weight and specific heat ratio.

14
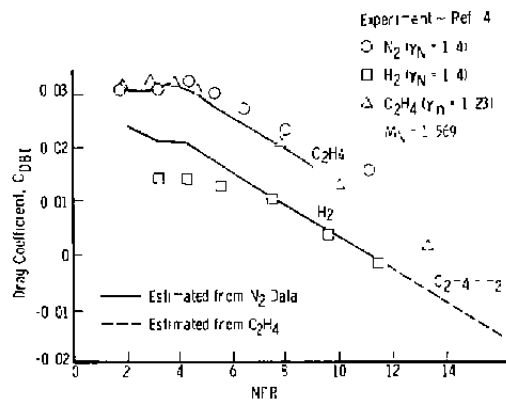
a. $M_\infty = 0.6$

b. $M_\infty = 0.9$

c. $M_\infty = 1.2$

Figure 3. Comparison with experiment of estimated drag for H_2 and C_2H_4 jets for the 15-deg AGARD afterbody.
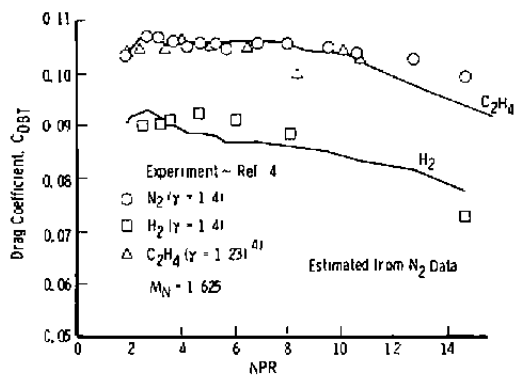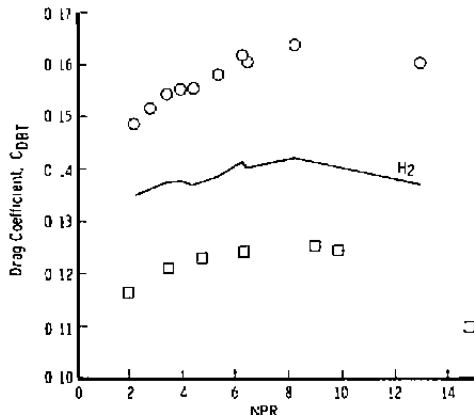
a. $M_\infty = 0.6$

b. $M_\infty = 0.9$

c. $M_\infty = 1.2$

Figure 4. Comparison with experiment of estimated drag for H_2 and C_2H_4 jets for the 25-deg AGARD afterbody.

3.3 EFFECT OF TOTAL TEMPERATURE AND RATIO OF SPECIFIC HEATS

The correlation method was applied to the data of Ref. 10 to predict the drag of a hot jet from the measured drag of a cold air jet. The hot jet was produced by burning ethylene (C_2H_4) with air; thus both the temperature and ratio of specific heats were different from cold air. The predicted results are compared with experiment as solid lines in Fig. 5 for the
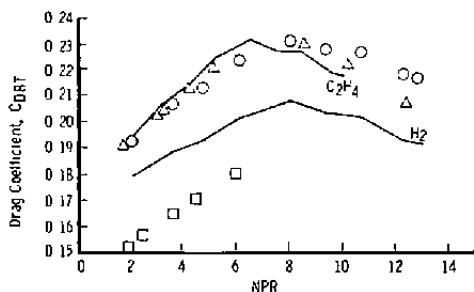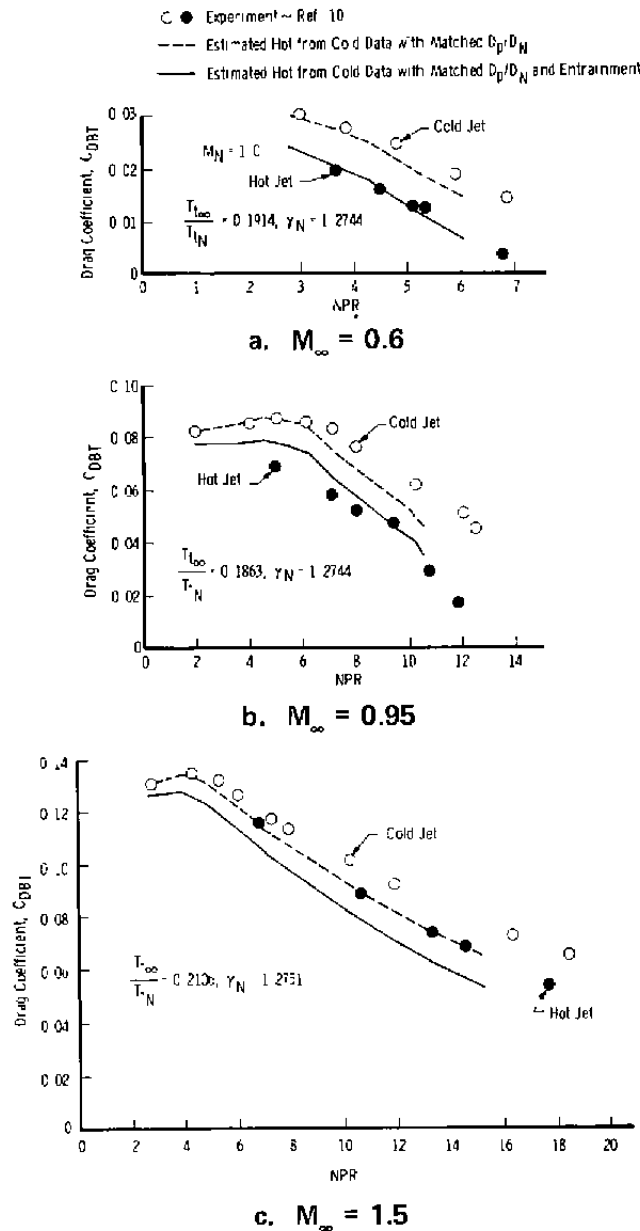

a. $M_\infty = 0.6$

b. $M_\infty = 0.95$

c. $M_\infty = 1.5$

Figure 5. Comparison with experiment of estimated drag for a hot jet from cold jet data for the 15-deg AGARD afterbody.

17

15-deg AGARD afterbody and in Fig. 6 for the 25-deg AGARD afterbody at Mach numbers of 0.6, 0.95, and 1.5, respectively. As shown for both afterbody configurations, the correlation method works extremely well at M_∞ = 0.6, underpredicts the induced drag at M_∞ = 0.95, and overpredicts the induced drag at M_∞ = 1.5. The difference between the predicted and experimental drag is partly due to neglecting, in the correlation method, the real gas effects and the jet total temperature gradient which occurred in the experiment. In addition, the correlation method does not account for spatial variations of the induced

a. M_∞ = 0.6

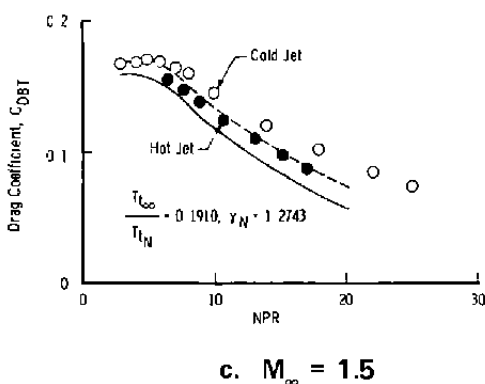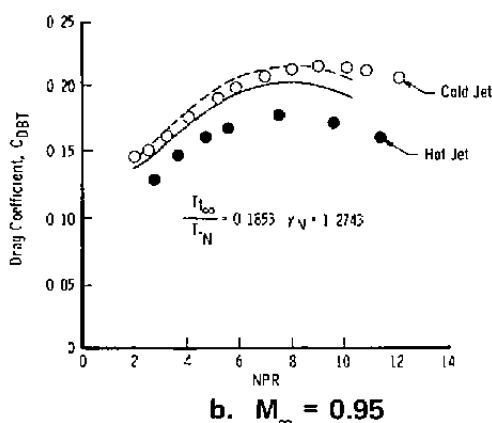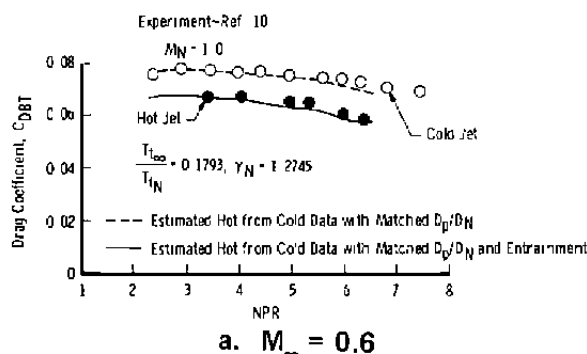b. M_∞ = 0.95

c. M_∞ = 1.5

Figure 6. Comparison with experiment of estimated drag for a hot jet from cold jet data for the 25-deg AGARD afterbody.

velocity which, no doubt, become important at $M_\infty = 1.5$. In spite of these deficiencies, the correlation method produces a significant improvement (except at $M_\infty = 1.5$) over merely using a correction for plume blockage, as is shown by the dashed line in Figs. 4 and 5.

The theory predicts that the induced velocity for a hot jet has the same direction as that for an H_2 jet, which, as previously discussed, results in a lower drag. This suggests that a cold, low molecular weight gas may be used to simulate the effects of a hot, relatively high molecular weight gas. A brief numerical study of the theoretical relation for the induced velocity, Eq. (18), revealed that, for a given γ_N, the induced velocity is only a function of the product $R_{g_N} T_{t_N}$. Since the induced velocity is a weak function of γ_N, then on the basis of the assumptions made, the two major parameters that affect afterbody body drag are $R_{g_N} T_{t_N}$ and D_p/D_N. Of course, there are minor effects caused by θ_N and $\Delta\nu$, as may be seen from Eq. (3).

3.4 EFFECT OF AREA RATIO, EXIT ANGLE, AND BLUNT BASE AREA

The purpose of this application of the correlation method is to illustrate the importance of maintaining the external afterbody geometry. The correlation method was applied to the data of Ref. 9 to predict the drag of two 15-deg AGARD afterbody configurations (one with and one without a blunt base) with $M_N = 1.0$ from the measured drag of a 15-deg AGARD afterbody without a blunt base having $M_N = 1.83$ and $\theta_N = 5$ deg. The predicted results are compared with experiment in Fig. 7 for $M_\infty = 0.6$ and 1.5. Only one theoretical result for both afterbodies is shown because the geometry differences are not sufficient to produce significantly different results. The predicted drag is in good agreement with experiment for the afterbody configuration without a blunt base, which is the same configuration used to obtain the reference drag data. The blunt base significantly increases the drag, and this cannot be accounted for by the present correlation method. However, the correlation method does apply to configurations having a blunt base since all of the previous data presented were from blunt base configurations. Geometric similarity must be maintained if the correlation method is to be valid.

3.5 EVALUATION OF CORRELATION METHOD

The improvement realized by using the correlation method was assessed by comparing the results with the two commonly used experimental correlation methods of matching NPR and D_P/D_N. For the free-stream Mach numbers considered, the accuracy of each correlation method was determined for two cases, $D_P/D_N \approx 1.0$, and its maximum value. The evaluations were made at Mach numbers of 0.6 and 1.2 for the N_2, H_2, and C_2H_4 data, and at 0.6, 0.95, and 1.5 for the hot jet data. In all, 15 evaluations were made for each afterbody

19

configuration. The results of this evaluation are presented in Table 1 for each afterbody configuration. As shown, the correlation method presented in this report (D_P/D_N + Entr) is from 50 to 60 percent more accurate than matching NPR and from 40 to 50 percent more accurate than matching D_p/D_N; also, the average predicted drag is within 10 percent of the correct value.

Experiment ~ Ref 10

○ $M_N = 1.8325$, $\theta_N = 5$ deg (No Base)

□ $M_N = 1.0$, $\theta_N = 0$ (With Base)

■ $M_N = 1.0$, $\theta_N = 0$ (No Base)

– – – Estimated $M_N = 1.0$ with Matched D_p/D_N

——— Estimated $M_N = 1.0$ with Matched D_p/D_N and Entrainment

a. $M_\infty = 0.6$

b. $M_\infty = 1.5$
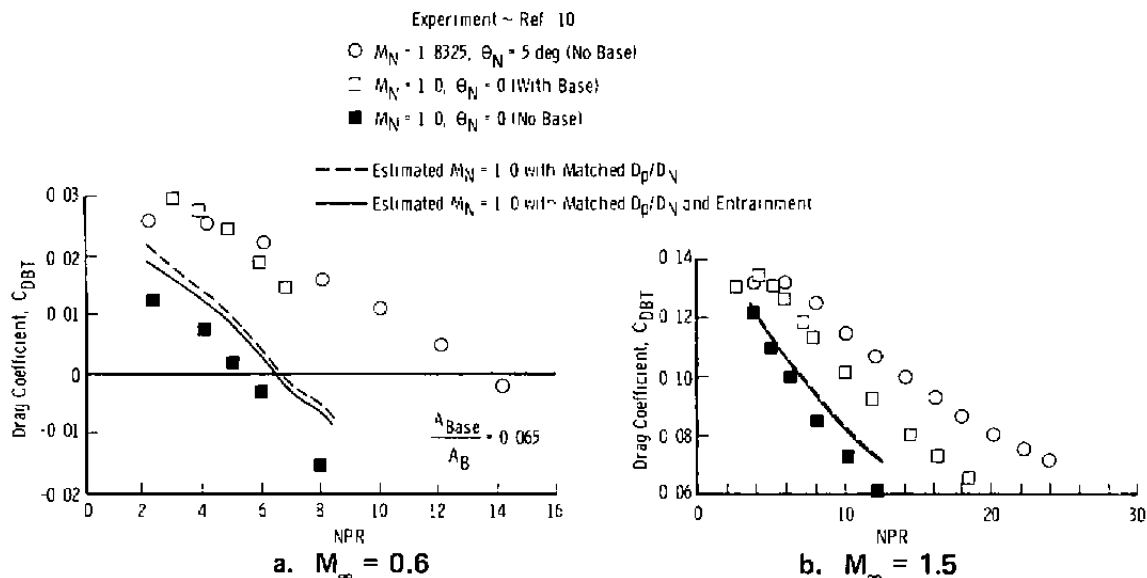
Figure 7. Comparison with experiment of estimated effects on drag of jet area ratio and blunt base area for the 15-deg AGARD afterbody.

Table 1. Evaluation of Correlation Methods

	Correlation Method			Average C_{DBT}
	NPR	D_p/D_N	D_p/D_N +Entr.	
I. 25° AGARD Afterbody				
1. Average absolute error, ΔC_{DBT}, over all conditions.	0.0173	0.0149	0.0081	0.1287
2. Percent error in predicted C_{DBT}	13.4%	11.6%	6.3%	
II. 15° AGARD Afterbody				
1. Average absolute error, ΔC_{DBT}, over all conditions.	0.0134	0.0120	0.0056	0.0603
2. Percent error In predicted C_{DBT}	22.2%	19.9%	9.3%	

20

4.0 SUMMARY OF RESULTS

The major results of this study are as follows:

1. The theoretical induced drag coefficient developed in this report provides a first-order estimate of the afterbody drag increments due to differences in jet mixing (entrainment) caused by different jet properties.

2. The correlation method used is:

   a. 40 to 50 percent more accurate than the correlation method based entirely on the blockage parameter,

   b. accurate to within 10 percent (average) for the two afterbody configurations considered in the Mach number range from 0.6 to 1.5,

   c. most accurate at Mach number 0.6 and least accurate in the Mach number range from 0.9 to 1.2, and

   d. relatively insensitive to the type of flow over the afterbody.

3. The theory indicates that the drag of a hot jet or H_2 jet is less than the drag of a cold air or N_2 jet because the jet mixing induced velocity is away from the jet plume boundary for the hot and H_2 jets and is toward the jet plume boundary for the cold air and N_2 jets. As a result, the flow over the afterbody is decelerated (decreased drag) by the jet mixing for the hot and H_2 jets and is accelerated (increased drag) by the jet mixing for the cold air and N_2 jets.

4. The theoretical induced drag is a strong function of the product $R_{g_N} T_{t_N}$ and a weak function of the ratio of specific heats, γ_N.

REFERENCES

1. Robinson, C. E. and High, M. D. "Exhaust Plume Temperature Effects on Nozzle Afterbody Performance Over the Transonic Mach Number Range." AEDC-TR-74-9 (AD781377), July 1974.

2. Compton, W. B. III. "Effects of Jet Exhaust Gas Properties on Exhaust Simulation and Afterbody Drag." NASA TR-R-444, October 1975.

3. Price, E. A. "A Parametric Investigation of the Annular Jet Concept for Obtaining Afterbody Drag Data at Transonic Mach Numbers." AEDC-TR-77-104 (ADA050891), February 1978.

4. Peters, W. L. "Jet Simulation Techniques: Simulation of Temperature Effects by Altering Gas Composition." AEDC-TR-78-43 (ADA067084), March 1979.

5. Yaros, S. F. "An Analysis of Transonic Viscous/Inviscid Interactions on Axisymmetric Bodies with Solid Stings or Real Plumes." AEDC-TR-77-106 (ADA050401), February 1978.

6. Fox, J. H. "A Generalized Base-Flow Analysis with Initial Boundary-Layer and Chemistry Effects." AEDC-TR-79-46 (ADA072683), July 1979.

7. Korst, H. H. and Chow, W. L. "Non-Isoenergetic Turbulent (P_{r_t} = 1.0) Jet Mixing Between Two Compressible Streams at Constant Pressure." ME-TN-393-2, Engineering Experiment Station, University of Illinois, Urbana, Illinois, April 1965.

8. Bauer, R. C. "An Analysis of Two-Dimensional Laminar and Turbulent Compressible Mixing." *AIAA Journal*, Vol. 4, No. 3, March 1966, pp. 392-395.

9. Tollmien, W. "Calculation of Turbulent Expansion Processes." NACA TM-1085, 1926.

10. Galigher, L. L., Yaros, S. F., and Bauer, R. C. "Evaluation of Boattail Geometry and Exhaust Plume Temperature Effects on Nozzle Afterbody Drag at Transonic Mach Numbers." AEDC-TR-76-102 (ADA030852), October 1976.

NOMENCLATURE

A   Area

b   Width of mixing zone

C   Crocco number

ΔC_{DB} Induced drag coefficient, i.e., entrainment drag

C_{DBO} Blockage drag coefficient, i.e., $\bar{\phi} = 0$

C_{DBT} Total afterbody pressure drag coefficient based on A_B

C_p Specific heat at constant pressure

D   Diameter

K   Constant in Prandtl's mixing length

k   Mass fraction

ℓ Prandtl's mixing length

M   Mach number

NPR   Nozzle pressure ratio, p_{t_N}/p_∞

P_t Total pressure

p   Static pressure

R_g Gas constant

r   Radius

T_t Total temperature

u   Velocity

u'   Small perturbation velocity parallel to the afterbody surface

v   Jet-mixing-induced velocity along free-stream edge of mixing zone

X   Distance from jet exit along inviscid jet boundary

Y   Mixing zone ordinate, positive toward the centerline

γ	Ratio of specific heats
η	Nondimensional mizing zone ordinate, $\sigma Y/X$
η_b	Nondimensional mixing zone width, $\sigma b/X$
η_m	η location of inviscid jet boundary
θ	Angle, Fig. 1
$\Delta\nu$	Prandtl-Meyer expansion angle at jet exit
ϱ	Density
σ	Similarity parameter for turbulent mixing
τ	Shear stress
ϕ	Nondimensional velocity, u/u_N
$\bar{\phi}$	Nondimensional induced velocity, Eq. (18)

SUBSCRIPTS

B	Afterbody
D	Dividing streamline
L	Low-speed edge of mixing zone
N	Jet or nozzle
P	Jet plume
U	High-speed edge of mixing zone
∞	Free stream